Waveguide Subsidiary Resonance Ferrite Limiters

JOSEPH HELSZAJN, MEMBER, IEEE, ROBERT W. MURRAY, E. G. S. DAVIDSON, AND ROBERT A. SUTTIE

Abstract—**This paper gives an analysis of *E*-plane waveguide ferrite limiters under subsidiary resonance conditions. Since Suhl's high-power damping term is power sensitive, it is necessary to evaluate it in every part of the ferrite structure before forming the dispersion relation. This is done in this paper by dividing the waveguide assembly in small elements transverse and parallel to the direction of propagation and calculating it in each region. The dispersion relation in each section along the direction of propagation is then formed in conjunction with the appropriate Suhl damping constant by establishing the transverse resonance condition. The total output power is obtained by forming the input/output relation for each section one at a time along the structure. The theory has been found useful in describing both the onset of limiting and the dynamic range of a ferrite limiter mounted on one of the narrow walls of the waveguide.**

Introduction

A NUMBER OF different waveguide ferrite limiters using *E*-plane structures under subsidiary resonance conditions [1]-[3] have been described in the literature [4]-[11]. All of these designs have relied on experiment for their adjustment. This paper permits the analysis of such limiters given the material parameters such as spinwave linewidth and magnetization, and the dimensions of the structure.

The complex propagation constant of such limiters is obtained by forming the dispersion relation in conjunction with Suhl's high-power damping constant [2]. Since this damping term is power sensitive, it is necessary to calculate it in every part of the ferrite. This is done by dividing the structure in elements transverse and parallel to the direction of propagation, and evaluating the circular magnetic field which establishes the subsidiary resonance in each region as a preliminary to calculating Suhl's damping term. The critical circular magnetic field is calculated from the magnetic variables of the ferrite material in the classical way. The dispersion relation of each section is then obtained one at a time by forming its overall *ABCD* matrix and applying the boundary conditions. The nonlinear attenuation for the first section is used to obtain the input/output relation for that section. The process is then repeated for the next one until the power transmitted by the last section gives the power transmitted by the device. Since all parts of this geometry do not have the same power, the dynamic range of such limiters is not limited to that of Suhl's high-power susceptibility, but it also is a function of the volume of the ferrite slab.

One arrangement considered in detail in this paper is that of a ferrite slab mounted on one of the narrow walls of the waveguide [4], [5]. The agreement between theory and experiment for this construction, while not complete, does appear to exhibit the general characteristics of this device.

The paper also includes some experimental work on a centrally located composite garnet-dielectric configuration, as well as on a laminar construction [10].

Manuscript received March 22, 1976; revised July 19, 1976. This work was supported by CVD under Contract CVD241.

J. Helszajn is with the Department of Electrical and Electronic Engineering, Heriot-Watt University, Edinburgh, Scotland.

R. W. Murray, E. G. S. Davidson, and R. A. Suttie are with the Microwave Development Laboratory, Ferranti Limited, Dundee, Scotland.

Complex Propagation Constant of *E*-Plane Waveguide Ferrite Limiter

The three important waveguide ferrite limiter configurations discussed in this paper are depicted in Fig. 1(a)-(c). The complex propagation constants of such structures can be obtained by evaluating their overall *ABCD* matrices and applying the boundary conditions at the waveguide walls. This is the standard approach to such problems and has been described in [12]-[15]. The overall matrix is constructed in terms of the individual matrices appropriate to each region. The three types of regions encountered in the theory of ferrite limiters are air, dielectric, and ferrite or garnet ones for which *ABCD* matrices are given in the Appendix. The ferrite regions in the transverse plane are further subdivided, and Suhl's high-power damping is introduced in each one of them. An additional geometry for which analysis is also possible is illustrated in Fig. 2. The overall *ABCD* matrix is obtained by matrix multiplication of the *ABCD* matrices of the individual regions in a straightforward manner.

$$\begin{bmatrix} A & B \\ C & D \end{bmatrix} = \begin{bmatrix} A_1 & B_1 \\ C_1 & D_1 \end{bmatrix} \begin{bmatrix} A_2 & B_2 \\ C_2 & D_2 \end{bmatrix} \begin{bmatrix} A_3 & B_3 \\ C_3 & D_3 \end{bmatrix} \cdots \begin{bmatrix} A_n & B_n \\ C_n & D_n \end{bmatrix}. \tag{1}$$

The *ABCD* matrix relates the electric and magnetic fields at the two waveguide walls

$$\begin{bmatrix} E_{z1} \\ H_{y1} \end{bmatrix} = \begin{bmatrix} A & B \\ C & D \end{bmatrix} \begin{bmatrix} E_{zn} \\ H_{yn} \end{bmatrix}. \tag{2}$$

Applying the boundary conditions $E_{z1} = E_{zn} = 0$ gives the dispersion relation from which γ is obtained. The result is $B = 0$.

Since the ferrite limiter is essentially a three-dimensional problem, the ferrite structure is now divided into small sections in the direction of propagation, and the dispersion relation found for each one, with the input power obtained by forming the input/output relation of the previous section.

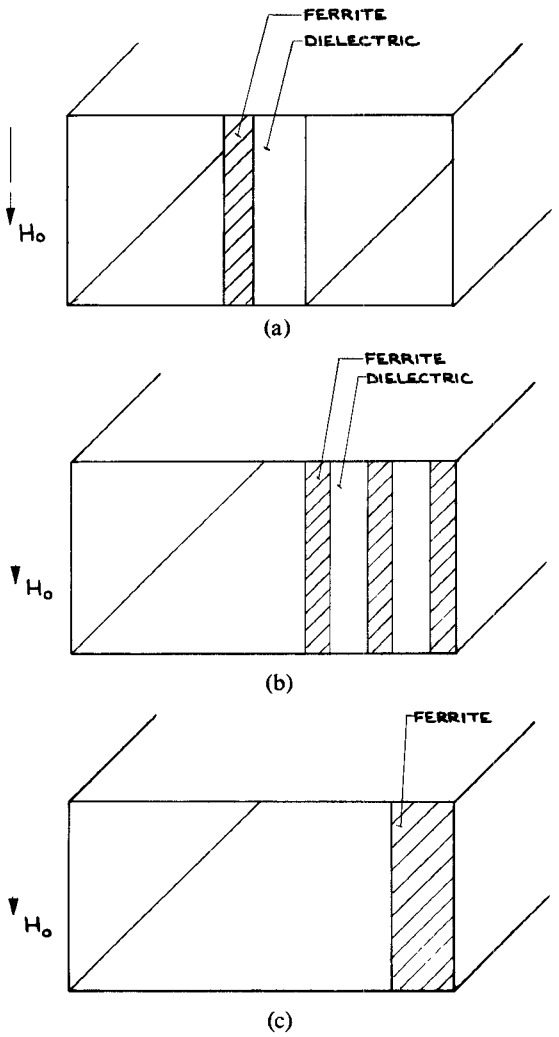

Fig. 1. (a) Schematic of composite garnet–dielectric limiter at center of waveguide. (b) Schematic of composite garnet–dielectric limiter mounted against narrow wall of waveguide. (c) Schematic of waveguide limiter using garnet slab against narrow wall of waveguide.

The schematic of the side mounted ferrite limiter is illustrated in Fig. 3.

Onset of Nonlinear Limiting Under Perpendicular Pumping

The onset of limiting under perpendicular pumping at the subsidiary resonance is described by the following standard relation [2]:

$$|h_+|_{crit} = \frac{\Delta H_k[(-\omega + \omega_r)^2 + \alpha^2\omega^2]^{1/2}}{\omega_m/\omega(\omega/2 + \omega_0 - N_z\omega_m)} \tag{3}$$

which gives the critical field for the circular polarization which establishes the subsidiary resonance.

The preceding equation applies at

$$\omega_k = \omega/2 \tag{4}$$

with $\theta_k = 45°$ and $k = 0$. In the preceding equations,

$$\alpha\omega = \gamma\Delta H/2 \tag{5}$$

$$\omega_k^2 = (\omega_0 - N_z\omega_m + \omega_m/2)(\omega_0 - N_z\omega_m) \tag{6}$$

$$\omega_r = (\omega_0 - N_z\omega_m) \tag{7}$$

and the other quantities have the usual meaning.

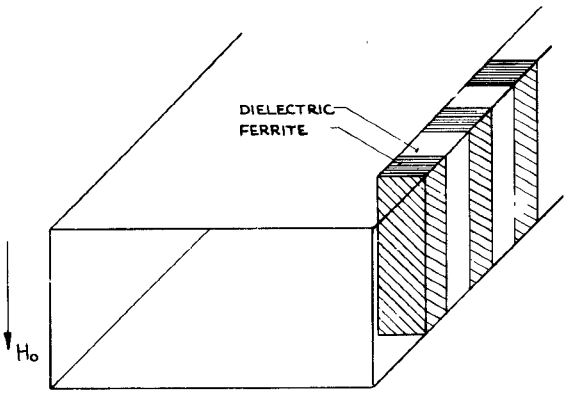

Fig. 2. Schematic of laminar limiter.

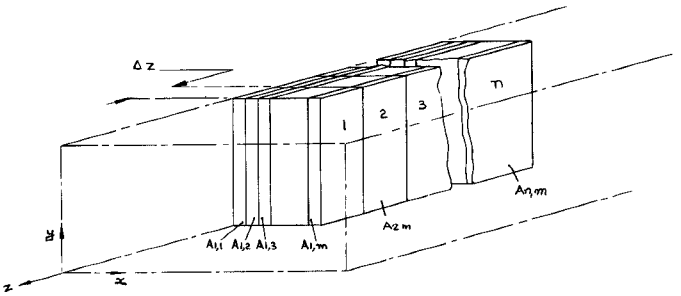

Fig. 3. Schematic of waveguide limiter indicating partitioning of device for computation purposes.

The value of the applied field H_0 at the subsidiary resonance is obtained by combining the preceding equations

$$(\omega/2)^2 = (\omega_0 - N_z\omega_m + \omega_m/2)(\omega_0 - N_z\omega_m). \tag{8}$$

Since only internal RF fields are used throughout this text, the preceding quantities do not involve the transverse demagnetizing factors N_x and N_y. A knowledge of N_z is also not necessary to evaluate $|h_+|_{crit}$ but is only required to calculate H_0 for experimental purposes.

Steady-State Susceptibility Under Conditions of Subsidiary Absorption

Below the onset of spinwave instability, the main effect of increasing the driving power is an increase in the amplitude of the uniform mode, or equivalently, an increase in the precession angle of the magnetization. Increasing the driving power above the critical threshold results in the transfer of power from the uniform mode to the spinwave modes, and the uniform mode remains constant just below its threshold value.

Therefore, above the critical threshold, the uniform mode saturates at the threshold value [2]

$$|m_+|_C^2 = \frac{\omega_m^2|h_+|^2}{(\omega - \omega_r)^2 + \Gamma^2}. \tag{9}$$

Below the critical threshold, the usual relation between m and h applies

$$|m_+|_C^2 = \frac{\omega_m^2|h_+|_C^2}{(\omega - \omega_r)^2 + \alpha^2\omega^2}. \tag{10}$$

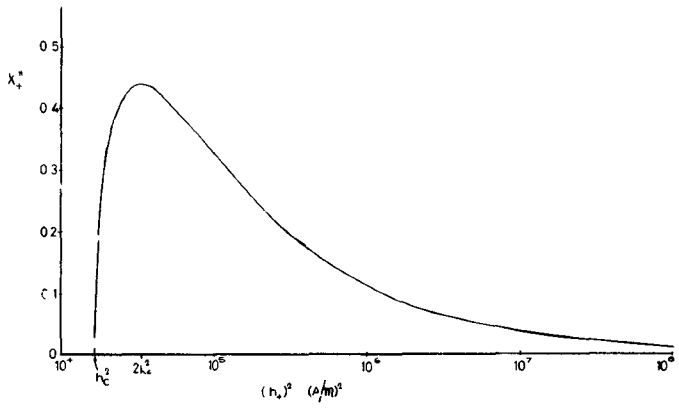

Fig. 4. High-power susceptibility versus circular magnetic field for pure YIG at 9.35 GHz.

Hence for $P > P_c$

$$\Gamma^2 = \frac{P}{P_c}\left[\alpha^2\omega^2 + (\omega - \omega_r)^2\right] - (\omega - \omega_r)^2 \quad (11)$$

where $P/P_c = h_+^2/h_{+c}^2$. The susceptibility above the critical power P_c at subsidiary resonance is given by

$$\chi_+(P > P_c) = \frac{\chi_+'}{P/P_c} - j\chi_+'' \cdot \frac{\sqrt{(\omega - \omega_r)^2(P/P_c - 1) + \alpha^2\omega^2 P/P_c}}{\alpha\omega P/P_c}. \quad (12)$$

If the subsidiary absorption resonance lies well below the main resonance, the imaginary part of the scalar susceptibility becomes

$$\frac{\chi_+''(P > P_c)}{\chi_+''} \approx \frac{1}{\alpha\omega} \cdot (\omega - \omega_r) \cdot \frac{\sqrt{P/P_c - 1}}{P/P_c}. \quad (13)$$

This equation increases from zero (since we have neglected the second term in the radicant) at $P = P_c$ to a maximum $(\omega - \omega_r)/2\alpha\omega$ at $P = 2P_c$, that is, 3 dB above critical power, and then steadily declines to zero. This is illustrated in Fig. 4.

This behavior suggests that every part of the ferrite should ideally operate under the condition $P/P_c = 2$. However, Fig. 4 indicates that effective limiting will occur provided the relative power lies between 1 and 10 dB above the critical power.

Tensor Permeability at High Power

One way the high-power circular susceptibility may be introduced into the tensor permeability is by writing the tensor elements μ and K in terms of the circular susceptibilities χ_+ and χ_-. The result is

$$\mu_+ = \mu - K = 1 + \chi_+ \quad (14)$$

$$\mu_- = \mu + K = 1 + \chi_-. \quad (15)$$

Combining the last two equations gives

$$\mu = 1 + \frac{(\chi_- + \chi_+)}{2} \quad (16)$$

$$K = \frac{(\chi_- - \chi_+)}{2} \quad (17)$$

where for $P > P_c$ the high-power damping term Γ is used in χ_+ instead of $\alpha\omega$. The complex circular susceptibilities are therefore given by

$$\chi_+(P > P_c) = \chi_+'(P > P_c) - j\chi_+''(P > P_c) = \frac{\omega_m}{-\omega + (\omega_r + j\Gamma)} \quad (18)$$

$$\chi_-(P > P_c) = \chi_-' - j\chi_-'' = \frac{\omega_m}{\omega + (\omega_r + j\alpha\omega)}. \quad (19)$$

The preceding quantities may now be used in conjunction with Maxwell's equations to obtain the high-power characteristic of the ferrite limiter.

The nonlinear Suhl's damping terms for the first section are

$$\Gamma_{1,1}^2 = \frac{h_{1,1}^2}{h_c^2}\left[\alpha^2\omega^2 + (\omega - \omega_r)^2\right] - (\omega - \omega_r)^2$$

$$\Gamma_{1,2}^2 = \frac{h_{1,2}^2}{h_c^2}\left[\alpha^2\omega^2 + (\omega - \omega_r)^2\right] - (\omega - \omega_r)^2$$

$$\Gamma_{1,m}^2 = \frac{h_{1,m}^2}{h_c^2}\left[\alpha^2\omega^2 + (\omega - \omega_r)^2\right] - (\omega - \omega_r)^2 \quad (20)$$

where $h_{1,1}, h_{1,2}, \cdots, h_{1,m}$ are the circular fields in the m elements of the first section with the total incident power being P W. Forming the dispersion relation for the first section now gives the power incident on the second section as

$$P - \Delta P_1 = Pe^{-2\gamma z} \quad (21)$$

where

$$\gamma = \alpha + j\beta \quad (22)$$

and α and β are the real and imaginary parts of the complex propagation constant γ. For the second section one has

$$\Gamma_{2,1}^2 = \frac{h_{2,1}^2}{h_c^2}\left[\alpha^2\omega^2 + (\omega - \omega_r)^2\right] - (\omega - \omega_r)^2$$

$$\Gamma_{2,2}^2 = \frac{h_{2,2}^2}{h_c^2}\left[\alpha^2\omega^2 + (\omega - \omega_r)^2\right] - (\omega - \omega_r)^2$$

$$\Gamma_{2,m}^2 = \frac{h_{2,m}^2}{h_c^2}\left[\alpha^2\omega^2 + (\omega - \omega_r)^2\right] - (\omega - \omega_r)^2 \quad (23)$$

where $h_{2,1}, h_{2,2}, \cdots, h_{2,m}$ are the circular fields in the m elements of the second section, with the total incident power being $P - \Delta P_1$. The program is complete when

$$(P - \Delta P_1 - \Delta P_2 \cdots) < P_c. \quad (24)$$

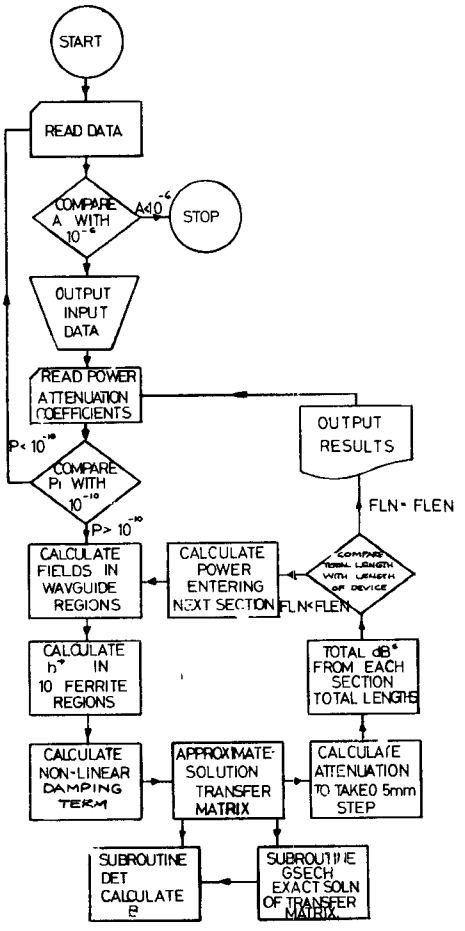

Fig. 5. Flow chart of computer program.

Computation

A flow diagram of the computer program used to analyze the *E*-plane ferrite limiters studied in this text is illustrated in Fig. 5. It is a modification of that used by Gardiol to permit the introduction of the nonlinear elements of the tensor permeability. In the arrangement used here the structure is divided into elements perpendicular and parallel to the direction of propagation. The ferrite region is partitioned into ten elements perpendicular to the direction of propagation and into $\frac{1}{2}$-mm-long sections along the direction of propagation. The dispersion relation is formed separately for each section in conjunction with the appropriate high-power susceptibilities. The nonlinear susceptibility in each element is obtained by calculating the circular magnetic field which establishes the subsidiary resonance in each region. The output power of the limiter is obtained by truncating (24).

The circular magnetic variable in these calculations is defined as

$$h_+ = \frac{h_x + jh_y}{2} \tag{25}$$

while the critical circular magnetic field is given by (3). In calculating the magnitude of the circular magnetic field in each section, it is assumed that both the output power and the attenuation coefficient of the previous section applies to it. Since only the low-power attenuation coefficient is available for the first section, its use leads to inconsistencies in that incorrect field patterns will be established in the first few sections. To avoid this difficulty, a separate program was written in which the computer cycles over the first section until a constant value of attenuation is obtained. Fig. 6 illustrates the variation of the attenuation coefficient with the number of cycles for different input powers.

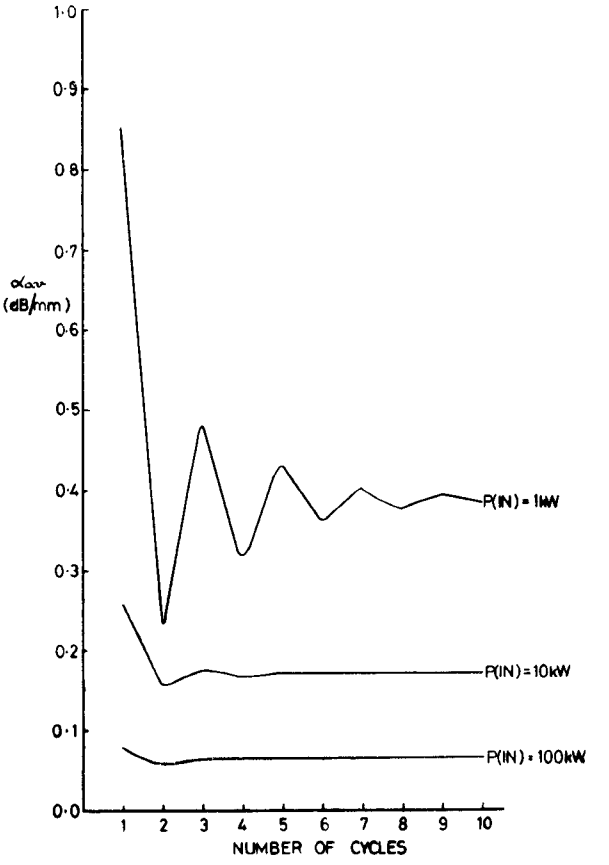

Fig. 6. First section attenuation constant for $W_f = 2.54$ mm.

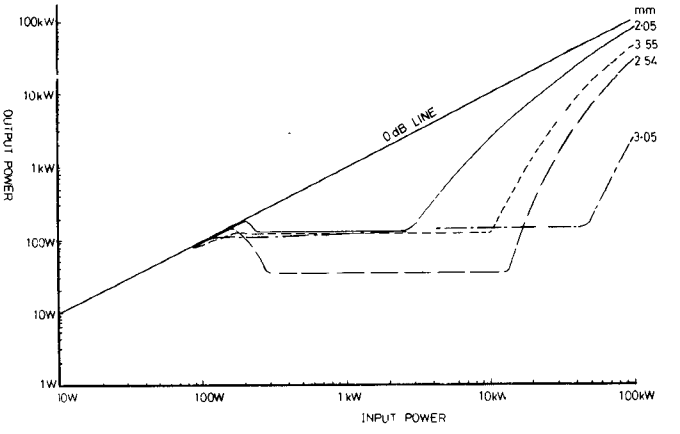

Fig. 7. Theoretical limiting characteristic for ferrite slab mounted against narrow wall of waveguide for W_f between 2 and 3.55 mm for 35-mm-long limiter.

Fig. 7 indicates the characteristics of *E*-plane limiters using garnet slabs mounted against the narrow wall of the waveguide in terms of their dimensions at 9.35 GHz. The garnet material used for these calculations is a pure YIG, for which $|h_+|_{crit}$ is given 129 A/m at 9.35 GHz.

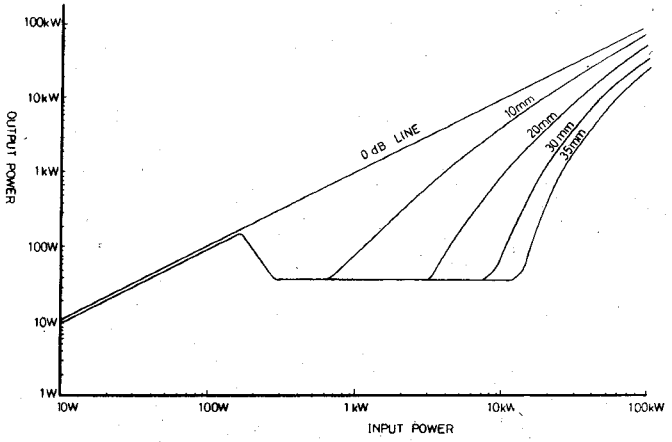

Fig. 8. Theoretical characteristic for ferrite slab mounted against narrow wall for the different lengths for $W_f = 2.54$ mm.

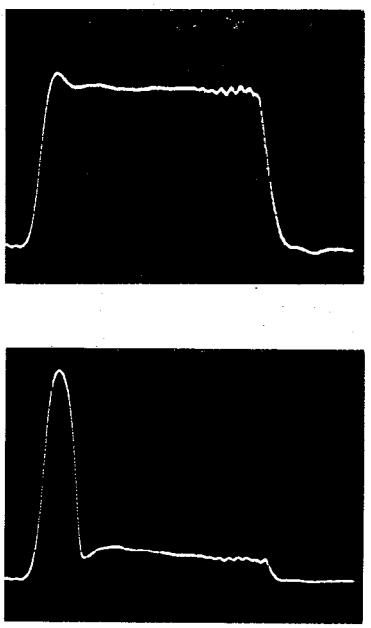

Fig. 9. Input and output pulses of subsidiary resonance limiter, with $P_{in} = 400$ W and $\tau = 0.65$ μs.

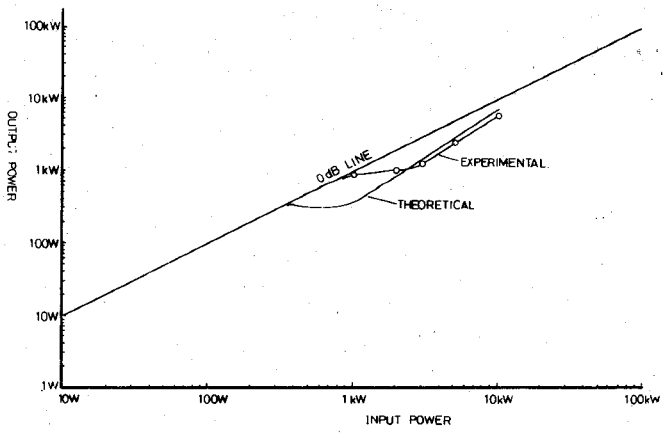

Fig. 10. Experimental limiter characteristic for garnet slab against narrow wall of waveguide for 35-mm-long limiter with $W_f = 1.52$ mm.

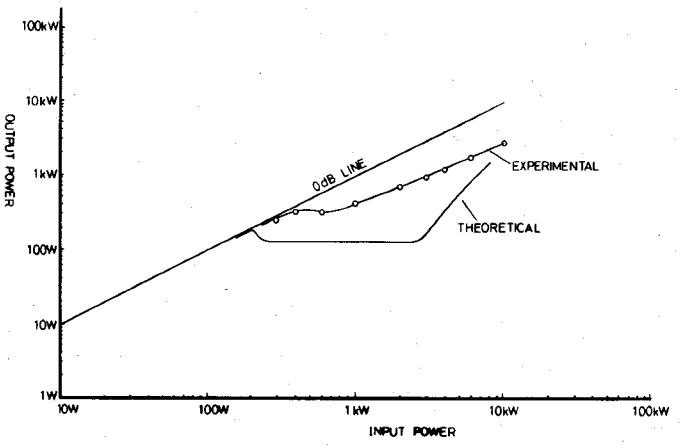

Fig. 11. Experimental limiter characteristic for garnet slab against narrow wall of waveguide for 35-mm-long limiter for $W_f = 2.05$ mm.

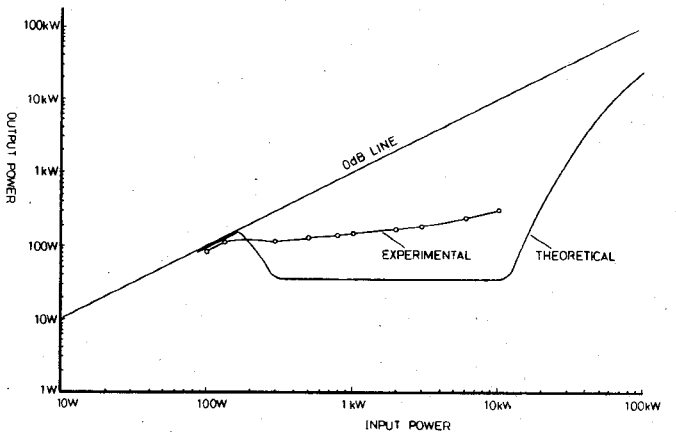

Fig. 12. Experimental limiter characteristic for garnet slab mounted against narrow wall of waveguide for 35-mm-long limiter for $W_f = 2.54$ mm.

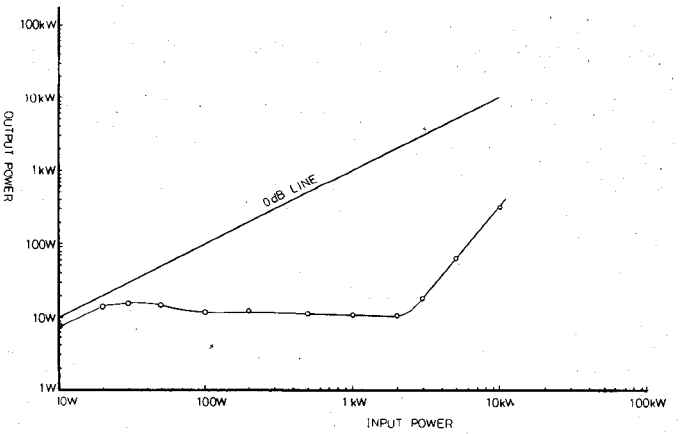

Fig. 13. Experimental limiter characteristics of garnet slab mounted against narrow wall of waveguide for 35-mm-long limiter at different magnetic fields for $W_f = 3.05$ mm.

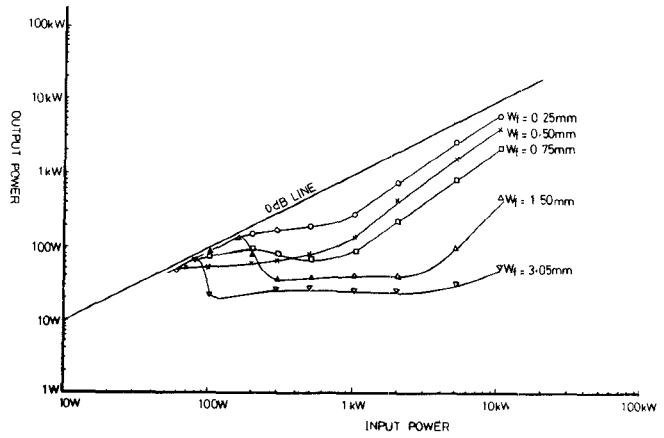

Fig. 14. Experimental limiter characteristic for a centrally located garnet–dielectric limiter with W_f + 3.05 mm for 35-mm-long limiter.

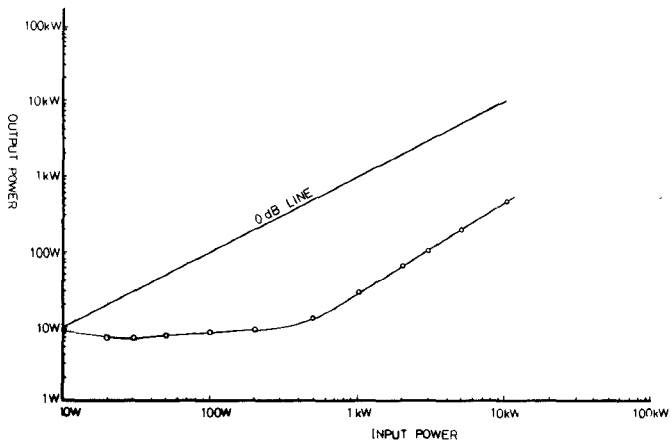

Fig. 15. Experimental characteristic of laminar limiter.

Fig. 8 gives the characteristic of one configuration as a function of the overall length of the device. It indicates that the limiting range of the limiter is essentially a function of its length. The fact that the flat region of some limiter configurations is less than the threshold value may be attributed to the real part of the circular susceptibility being power sensitive as well as the imaginary component.

High-Power Characteristics of Ferrite Limiters

This section presents some experimental results obtained on the limiter geometries depicted in Figs. 1(a) and (c) and 2. All the limiters described here use polycrystalline YIG with $\Delta H_k = 114$ A/m[1] and a magnetization of $M_0 = 0.1780$ Wb/m^2. The experimental arrangement employed a calibrated bypass channel so that both the incident and output signals of the limiter could be readily monitored. Fig. 9 illustrates the output pulse which consists of the characteristic initial spike region due to the finite time required to initiate subsidiary resonance, followed by the flat portion which applies in the limiting region. All measurements were made using a tunable X-band magnetron at a fixed frequency of 9.35 GHz. The peak power with a pulsewidth of 1.0 μs and a pulse-repetition frequency of 1000 Hz was varied 0–10 kW.

Figs. 10–12 depict limiting characteristics for the configuration illustrated in Fig. 1(c) for $W_f = 1.5$, 2.05, and 2.54 mm. It shows the influence of the garnet thickness on the onset of limiting and the dynamic range for a limiter 35 mm long. Fig. 13 indicates the input/output relation for the same arrangement with $W_f = 3.05$ mm. The characteristic for this limiter is not unique in that it is strongly influenced by the direct magnetic field. Although the limiting threshold achieved here is compatible with the lowest threshold obtained, theoretically the small-signal characteristic of this device exhibited large variation in its insertion loss with frequency.

Fig. 14 depicts the input/output relations for the limiter illustrated in Fig. 1(a). In this arrangement, the overall width of the transverse assembly was kept constant at 3.05 mm while the garnet thickness W_f was altered. The main section of the limiter was 35 mm long with 18-mm-long tapers at each end for matching purposes.

Fig. 15 illustrates the limiting characteristic of the laminar construction in Fig. 2. The assembly used here consisted of six garnet rods spaced by five alumina rods of the same cross section, the cross section of the rods being 3.0 × 3.0 mm. The total length of this device was 33 mm long, but its effective length was half this value since the dielectric spacers do not contribute to the limiting. The dynamic range for this device is by far the smallest of those studied, which is consistent with the fact that its effective length is the shortest. The insertion loss of the experimental limiters was typically $\frac{1}{2}$ dB in each instance.

Conclusion

This paper has described the analysis of E-plane waveguide ferrite limiters. The theory has been found useful in investigating the onset of limiting and the dynamic range of a ferrite slab limiter configuration. Such experimental limiters have also been constructed and evaluated. One feature of these limiters is that their limiting thresholds and dynamic ranges appear to be a function of the garnet volume rather than of their location in the waveguide. The analysis applies, provided the ferrite loaded waveguide does not propagate the TE_{20} mode.

Appendix

ABCD Matrices of Standard Waveguide Regions

The *ABCD* matrices for the three standard regions encountered in this paper are listed as follows. In the ferrite region, the *ABCD* matrix is defined by

$$A = \cos k_m\delta_m + j\frac{\gamma}{k_m}\left(\frac{K}{\mu}\right)\cdot \sin k_m\delta_m$$

$$B = -\frac{j\omega\mu_0\mu_e}{k_m}\sin k_m\delta_m$$

$$C = -\frac{jk_m}{\omega\mu_0\mu_e}\left(\frac{-\gamma^2}{k_m{}^2}\frac{K^2}{\mu^2} + 1\right)\sin k_m\delta_m$$

$$D = \cos k_m\delta_m - j\frac{\gamma}{k_m}\left(\frac{K}{\mu}\right)\sin k_m\delta_m$$

[1] It is observed that the value for ΔH_k used here applies to a parallel pump arrangement while the experimental geometry described in this text is a perpendicular pump arrangement.

where

$$k_m^2 = \omega^2 \mu_0 \varepsilon_0 \mu_e \varepsilon_r + \gamma^2$$

$$\mu_e = \frac{\mu^2 - K^2}{\mu}$$

and δ_m is the width of the ferrite region.

If the direction of the magnetic field is reversed, the sign of K/μ is changed in the preceding equations. In the air region, the $ABCD$ matrix is

$$A = \cos k\delta$$

$$B = -\frac{j\omega\mu_0}{k} \sin k\delta$$

$$C = -\frac{jk}{\omega\mu_0} \sin k\delta$$

$$D = \cos k\delta$$

where

$$k^2 = \omega^2 \varepsilon_0 \mu_0 + \gamma^2$$

and δ is the width of the air region, while for the dielectric region it is

$$A = \cos k_d \delta_d$$

$$B = \frac{-j\omega\mu_0}{k_d} \sin k_d \delta_d$$

$$C = \frac{-jk_d}{\omega\mu_0} \cdot \sin k_d \delta_d$$

$$D = \cos k_d \delta_d$$

where

$$k_d^2 = \omega^2 \mu_0 \varepsilon_0 \varepsilon_d + \gamma^2$$

and δ_d is the width of the dielectric region.

Acknowledgment

The authors wish to thank Dr. J. Clark and M. Dunsmore of the Royal Radar Establishment for many helpful discussions.

References

[1] R. W. Damon, "Relaxation effects in the ferromagnetic resonance," *Rev. Mod. Phys.*, vol. 25. pp. 239–245, Jan. 1953.
[2] H. Suhl, "The nonlinear behavior of ferrites at high microwave signal levels," *Proc. IRE*, vol. 44, pp. 1270–1284, Oct. 1956.
[3] J. Helszajn, "Simplified theory of nonlinear phenomena in ferrimagnetic materials," *Proc. IEE*, vol. 114, Nov. 1967.
[4] R. L. Martin, "High power effects in ferrite slabs at *X*-band," *J. Appl. Phys.*, suppl. to vol. 30, pp. 1595–1605, Apr. 1959.
[5] G. S. Uebele, "Characteristics of ferrite microwave limiters," *IRE Trans. Microwave Theory Tech.*, vol. MTT-7, pp. 18–23, Jan. 1959.
[6] W. F. Krupke, T. A. Hartwick, and M. T. Weiss, "Solid-state *X*-band power limiter," *IRE Trans. Microwave Theory Tech.*, vol. MTT-9, pp. 472–480, Nov. 1961.
[7] J. Brown, "Ferromagnetic limiters," *Microwave J.*, vol. 4. p. 74, Nov. 1961.
[8] J. L. Carter and J. W. McGowan, "*X*-band ferrite-varactor limiter," *IEEE Trans. Microwave Theory Tech.* (Corresp.), vol. MTT-17, pp. 231–232, Apr. 1969.
[9] J. L. Allen, "A compact subsidiary resonance limiter," *IEEE Trans. Microwave Theory Tech.*, vol. MTT-20, pp. 193–231, Feb. 1972.
[10] J. L. Carter and J. W. McGowan, "A laminar subsidiary resonance limiter," *IEEE Trans. Microwave Theory Tech.*, vol. MTT-18, pp. 652–654, Sept. 1970.
[11] H. S. Maddix and R. Kalvaitis, "Ferrite diode limiters for *S*, *X* and K_u bands," European Microwave Conf., Stockholm, Sweden, Aug. 1971.
[12] W. P. Clark, K. H. Hering, and D. A. Charlton, "TE-mode solutions for partially ferrite filled rectangular waveguide using *ABCD* matrices," *IEEE Int. Convention Record* (U.S.A.), vol. 14, pp. 15, 39–48, 1966.
[13] F. E. Gardiol and A. S. Vander-Vorst, "Computer analysis of *E*-plane resonance isolators," *IEEE Trans. Microwave Theory Tech.*, vol. MTT-19, pp. 315–322, Mar. 1971.
[14] M. C. Decreton *et al.*, "Computer optimisation of *E*-plane resonance isolators," *IEEE Trans. Microwave Theory Tech.*, vol. MTT-19, pp. 322–331, Mar. 1971.
[15] P. J. B. Clarricoats, *Microwave Ferrites*. London: Chapman Hall, 1961.